Exchange-induced Tm magnetism in multiferroic h-$TmMnO_3$

2009 J. Phys.: Condens. Matter 21 386001

(http://iopscience.iop.org/0953-8984/21/38/386001)

J. Phys.: Condens. Matter **21** (2009) 386001 (5pp) doi:10.1088/0953-8984/21/38/386001

Exchange-induced Tm magnetism in multiferroic h-$TmMnO_3$

Hazar A Salama and G A Stewart

School of Physical, Environmental and Mathematical Sciences, University of New South Wales, Australian Defence Force Academy, Canberra 2600, Australia

Received 4 June 2009, in final form 10 August 2009
Published 24 August 2009
Online at stacks.iop.org/JPhysCM/21/386001

Abstract

Analysis of ^{169}Tm Mössbauer spectra recorded for (hexagonal phase) h-$TmMnO_3$ confirms that the Mn sublattice orders magnetically below $T_N^{Mn} = 82$–83 K and reveals the growth of a local Tm moment at the 4b site that is induced by the Mn–Tm exchange interaction. The maximum hyperfine field recorded at the ^{169}Tm nucleus is 312 T, which is just under half of the free ion value and corresponds to a saturation moment of 3.29 μ_B. The temperature dependence of the fitted magnetic hyperfine interaction is closely represented by a simple two-singlet ground state model for the Tm^{3+} crystal field scheme. The saturation molecular field is deduced to lie in the range $B_{Mn-Tm}(T = 0\ K) = 1.2$–$2.3$ T, dependent on the expectation value of the coupling $\alpha = \langle 0|J_z|1\rangle$ between the two-singlet states. As observed elsewhere for other hexagonal manganites, there is no Mn-based exchange field at the second Tm site (the 2a site) which contributes a paramagnetic subspectrum down to the lowest experimental temperature of 4.2 K.

(Some figures in this article are in colour only in the electronic version)

1. Introduction

Rare earth manganites, $RMnO_3$ (R = rare earth), continue to attract considerable interest because of their diverse range of physical properties. They can be divided into two groups depending on the R^{3+} ionic radius. For larger radii (R = La → Dy) the orthorhombic structure is stabilized. However, for the smaller ions (R = Y, Ho → Lu) the hexagonal (h) $LuMnO_3$-type structure is obtained with the space group $P6_3cm$ [1]. The h-$RMnO_3$ are currently under intense scrutiny because of their multiferroic behaviour. Typically, they undergo both a ferroelectric transition at $T_C^{Mn} \approx 1000$ K and an antiferromagnetic transition at a lower temperature ($T_N^{Mn} \approx 100$ K) due to strong couplings between the Mn ions (Huang *et al* [2] and references therein). Below T_N^{Mn}, the geometrical frustration [3] is broken by the within-plane, Mn–O–Mn superexchange that leads to a 120° arrangement of Mn spins. According to the B-type triangular ordering determined by Fiebig *et al* [4], there is an additional weaker antiferromagnetic coupling between the planes at $z = 0$ and 1/2. The rare earth sites eventually order in their own right at much lower temperatures. For example, independent ^{170}Yb Mössbauer investigations of the neighbouring h-$YbMnO_3$ recently reported ordering temperatures of $T_N^{Yb} = 3.5$ K [5] and 5 K [6] in close agreement with a value of 4 K determined using dielectric measurements [7]. However, the Mn–Yb exchange interaction was observed to induce a moment on the Yb 4b site at temperatures well above T_N^{Yb}. With the assistance of complementary neutron diffraction data, Fabrèges *et al* [5] were able to describe the evolution of this moment in terms of the Mn–Yb exchange acting on a Kramers doublet ground state of the Yb^{3+} crystal field (CF) scheme.

In the case of the ^{170}Yb Mössbauer measurements, the spectra were complicated by paramagnetic relaxation of the Yb^{3+} Kramers doublets. Furthermore, the small recoil-free fraction of the ^{170}Yb 84.25 keV Mössbauer resonance restricted the measurements to a maximum temperature of about 40 K. In this present work, we have therefore employed the ^{169}Tm Mössbauer resonance ($I_e = 3/2$, $I_g = 1/2$, $E_\gamma(E1) = 8.4$ keV) to investigate the exchange-induced magnetic behaviour of the Tm^{3+} ions in h-$TmMnO_3$ over the full temperature range of $4.2\ K < T < T_N^{Mn}$. The advantage of the ^{169}Tm 8.4 keV resonance is that spectra can be recorded to temperatures well above room temperature. Using bulk magnetization methods, the Néel temperature for h-$TmMnO_3$ has been reported elsewhere in the literature as $T_N^{Mn} = 84$ K [7] and 82 K [8] for single-crystal specimens and 81 K [9] for a powdered specimen, with $T_N^{Tm} < 1.8$ K [7].

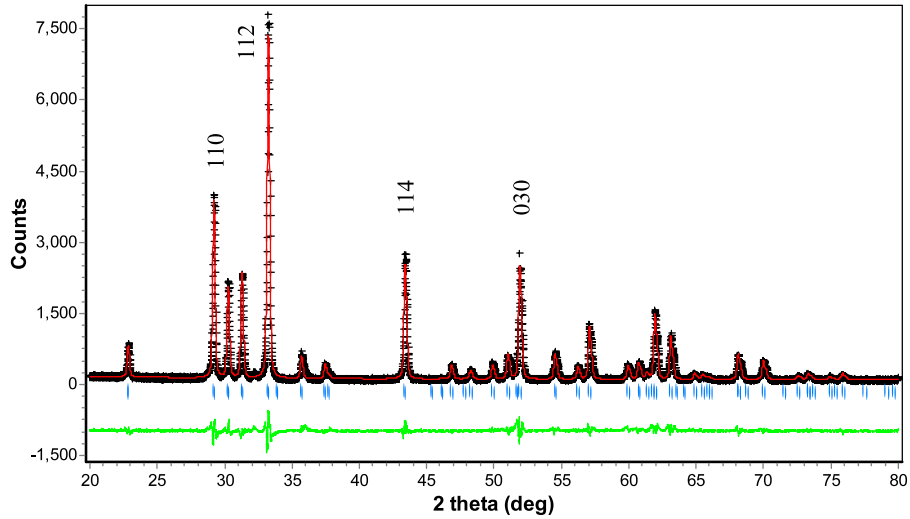

Figure 1. X-ray powder diffraction pattern for h-$TmMnO_3$. The diffraction data are given as crosses and the solid curve through the data corresponds to the fitted theory. Below the pattern, there are individual reflection markers and the curve indicates the difference between the observed data and the fit.

2. Experimental details

A polycrystalline specimen of h-$TmMnO_3$ was prepared from stoichiometric amounts of Tm_2O_3 (99.9%) and $MnCO_3$ (99.9%). The materials were mixed intimately using a mortar and pestle, pressed into a pill, and heated in air at 1250 °C for 16 h. This process was repeated three times. For the first heat treatment cycle, the temperature was held at 900 °C for 1 h before proceeding to 1250 °C. The purpose of this was to allow the expelled CO_2 to diffuse gently out of the pellet. The x-ray powder diffraction pattern (figure 1) recorded using Cu Kα radiation was consistent with a single hexagonal phase. The solid curve drawn through the data in figure 1 was fitted using *Rietica* [10]. It corresponds to lattice parameters of $a = 0.60799(5)$ nm and $c = 1.13754(4)$ nm which are in close agreement with those reported elsewhere [8, 9, 11].

For the ^{169}Tm Mössbauer spectrum acquisition, the specimen absorber ($\approx$9 mg cm^{-2}) was mounted vertically inside a helium cryostat and the ^{169}Er:^{168}Er (10 wt.%)Al source was mounted on an external sinusoidal motion drive whose velocity was calibrated against the spectrum for TmF_3.

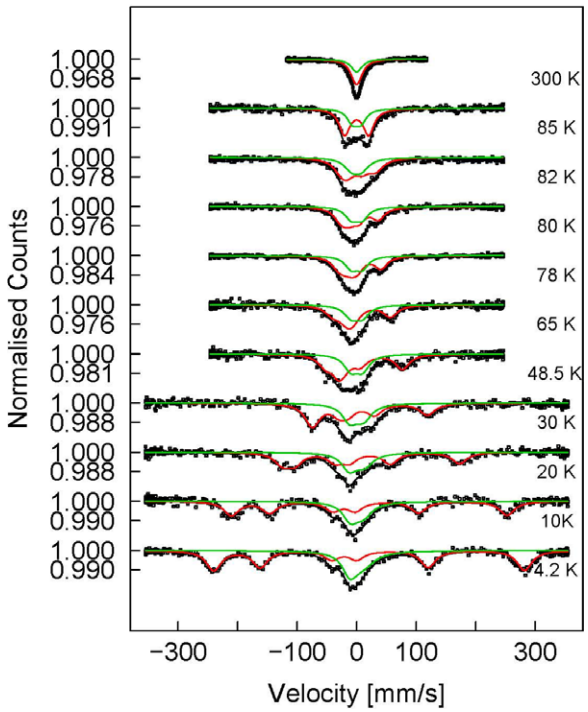

Figure 2. Representative ^{169}Tm Mössbauer spectra for h-$TmMnO_3$. The fitted theory curve is the sum of a magnetic sextet (red on-line) and an asymmetric doublet (green on-line) corresponding to the Tm 4b and 2a sites, respectively.

3. Results and discussion

The ^{169}Tm Mössbauer spectra recorded for h-$TmMnO_3$ are presented in figure 2. There is evidence of magnetic splitting over a wide temperature range and all of the spectra were able to be fitted with the superposition of a magnetic sextet and a quadrupole-split doublet in the intensity ratio of 2:1. This confirms that the Mn–Tm exchange interaction acts only at the more prevalent Tm 4b site. A similar observation was made in the case of h-$YbMnO_3$ via both infra-red spectroscopy [12, 13] and ^{170}Yb Mössbauer spectroscopy [5, 6, 14]. The magnetic moment induced on the Tm^{3+} 4b site and the associated hyperfine field, B_{hf}, acting at its ^{169}Tm nucleus are expected to align with the c-axis. This is because the triangular arrangements of Mn spins in the layers above and below combine to produce a molecular field acting along the c-axis (as discussed in the early infra-red spectroscopy work of Kritayakirana *et al* [12]). Based on symmetry arguments, the c-axis is also expected to be the principal z-axis of the total electric field gradient (efg) tensor acting at the nucleus. Although the 4b site symmetry of 3 (C_3) allows for a non-zero asymmetry parameter, the 2a site symmetry of 3m (C_{3v})

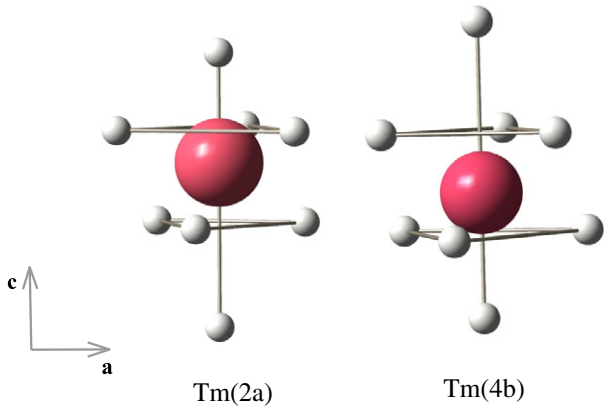

Figure 3. The two Tm site configurations in h-$TmMnO_3$.

does not. However, the two sites have very similar local environments (figure 3) so that we might expect the asymmetry parameter to be negligible for the 4b site. This approach was employed successfully with the analyses of magnetic ^{170}Yb spectra for h-$YbMnO_3$ [6, 14]. For these reasons, the magnetic sextet in this present work was analysed in terms of a simple coaxial nuclear Hamiltonian of the form

$$\mathcal{H}_N = a(I)I_z + \frac{P}{3}[3I_z^2 - I(I+1)] \qquad (1)$$

where $P = 3eQV_{zz}/4I(2I-1)$ is the quadrupole hyperfine parameter for the excited ($I_e = 3/2$) level and $a(I) = \mu(I)B_{hf}/I$ are the Zeeman hyperfine parameters with $a(I_e = 3/2)/a(I_g = 1/2) = 0.741(4)$ [15]. In the case of ^{169}Tm Mössbauer spectroscopy, the analysis is already simplified by the fact that the isomer shift is negligible and is set to zero [16]. In addition, the spectra were first fitted under the strict conditions that all absorption lines have the same Lorentzian width with relative intensities of 3:2:1:1:2:3 for the magnetic sextet and 1:1 for the paramagnetic doublet. However, in the case of the lower measurement temperatures (4.2, 10, 20 and 30 K), it was found necessary to relax the relative intensity condition for the magnetic sextet and to allow the positive velocity absorption line of the doublet to have a marginally larger line width. It is not clear to the authors why the central lines of the magnetic sextet are slightly more intense than expected but the broadened doublet line is a relaxation effect that is often observed for paramagnetic Tm sites.

The analysis of the 4.2 K spectrum yielded $a(1/2) = 162.1(1)$ mm s^{-1} for the 4b site. Using the nuclear magnetic moment value of $\mu(1/2) = -0.2310(15)\ \mu_N$ [17], this converts to $B_{hf} = 311.8(2)$ T. Furthermore, if extra-ionic contributions can be ignored, then B_{hf} is proportional to the thermal average of the local Tm^{3+} moment so that

$$\frac{B_{hf}}{B_{hf}(FI)} = \frac{\langle J_z\rangle}{J} = \frac{\langle \mu_z\rangle}{\mu_z(FI)} \qquad (2)$$

where the 'free ion' values are $B_{hf}(FI) = 662.5$ T [18] and $\mu_z(FI) = g_J J = 7\ \mu_B$. Under this assumption the fitted value of B_{hf} corresponds to a local 4b site moment of $\mu_z \approx 3.29(1)\ \mu_B$. This is approximately 47% of the maximum free ion moment of 7 μ_B and is indicative of significant CF quenching.

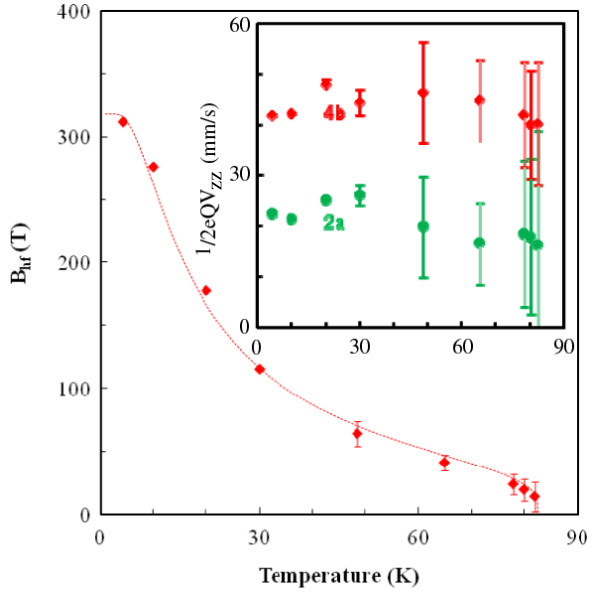

Figure 4. Temperature dependence of the ^{169}Tm hyperfine field, B_{hf}, at the 4b site of h-$TmMnO_3$. The fitted theory curve is based on a simple two-singlet CF ground state model (see text) with $\alpha = 6$, $\Delta = 20$ K and a saturation Mn–Tm molecular field of B_M(Mn–Tm) = 1.27 T. The temperature dependence of the quadrupole interaction, $\frac{1}{2}eQV_{zz}$, is shown in the inset for both the 4b site (solid diamonds) and the 2a site (solid circles).

The fitted quadrupole interaction parameters yielded $\frac{1}{2}eQV_{zz} = 41.9$ (2) mm s^{-1} and 22.3(4) mm s^{-1}, respectively for the 4b and 2a sites. Again, if we ignore the lattice contributions, these values are significantly smaller than the free ion, 4f-shell contribution of $\frac{1}{2}eQV_{zz}^{4f}$ (FI) = 58.6 mm s^{-1} (with $Q = -1.5$ b [19] and V_{zz}^{4f} (FI) $= -69 \times 10^{21}$ V m^{-2} [18]). The fact that the quadrupole interaction strength measured for the 4b site sextet is about twice that measured for the 2a site doublet implies that the local environments might not be as similar as we had expected.

With increasing temperature the magnetic splitting of the 4b site collapses and eventually vanishes at 82–83 K which is in good agreement with the values of $T_N^{Mn} \approx 81$–84 K reported elsewhere for h-$TmMnO_3$ [7–9]. The fitted B_{hf} values are shown as a function of temperature in figure 4 and the fitted quadrupole interactions are shown in the figure's inset. As the spectrum collapses the individual transition lines are less well resolved, leading to increased experimental uncertainties at higher temperatures. Nevertheless, the quadrupole interactions appear to be temperature independent over the full range of temperature that is associated with the Mn magnetization. This observation supports the well-isolated CF ground state model that is proposed in the next section. If only the same lowest energy states are thermally populated, then the 4f-shell contribution to the quadrupole interaction at the ^{169}Tm nucleus is expected not to vary with temperature. It is interesting that Yen *et al* [7] detected the onset of the antiferromagnetic order of the Mn sublattice via its influence on the dielectric constant [7]. That is, it was detected via the coupling between

Table 1. CF parameter estimates for the Tm 4b site of h-$TmMnO_3$. The Stevens operator equivalent notation is employed.

	PCM calculations		Converted from
	$r \geqslant 50\ a$[a]	R_z (65.3°)[b]	h-$YbMnO_3$[c]
B_2^0 (mK)	−3.86	−3.86	−2.11
B_4^0 (mK)	−3.36	−3.36	−1.83
B_4^3 (K)	−0.609	+0.633	+1.37
B_4^{-3} (K)	−0.173	Zero	Zero
B_6^0 (mK)	−0.107	−0.107	−0.389
B_6^3 (mK)	−0.899	+0.923	+2.59
B_6^{-3} (mK)	−0.215	−0.039	Zero
B_6^6 (mK)	−0.846	−0.907	−4.41
B_6^{-6} (mK)	−0.356	+0.143	Zero

[a] For Tm^{3+}, Mn^{3+}, O^{2-} with $(x, y, z)_{CF} \parallel (a, b, c)$ and atomic position parameters taken from Uusi-Esko *et al* [9].

[b] Coordinate rotation about z-axis to achieve $B_4^{-3} = 0$ K in new frame.

[c] Converted from experimental results for h-$YbMnO_3$ [13].

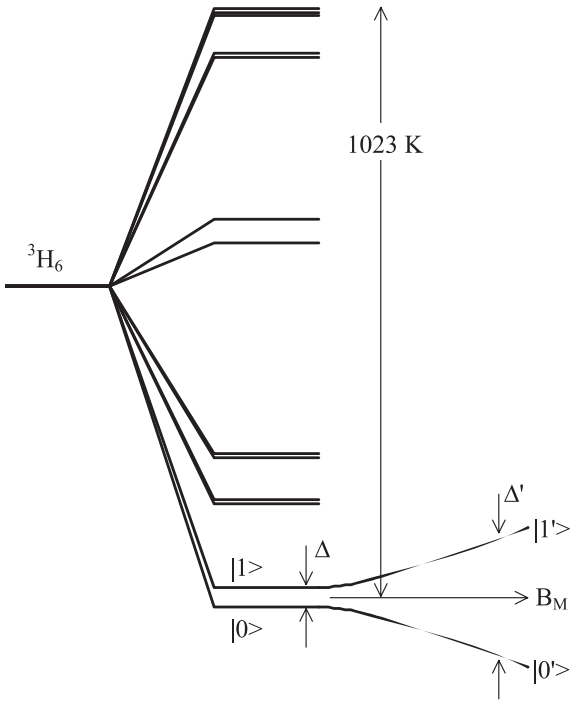

Figure 5. Tentative CF scheme for the Tm^{3+} ion at the 4b site in $TmMnO_3$, based on CF parameters converted from those reported for h-$YbMnO_3$ by Diviš *et al* [13]. The influence of a molecular field arising out of the Mn–Tm exchange interaction is shown schematically with an exaggerated increase in the energy separation of the two-singlet states $|0\rangle$ and $|1\rangle$.

the magnetic and ferroelectric states. However, in this present work there is no discernible impact on the ^{169}Tm quadrupole interaction. In particular, the value of $\frac{1}{2}eQV_{zz}^{4f}$ at the 4b site nucleus is constant over the temperature range of 80–85 K.

4. Crystal field theory model for the induced Tm^{3+} moment on the 4b site

The hexagonal $RMnO_3$ structure consists of MnO_5 bipyramids stacked in layers alternating with layers of R^{3+} ions. As mentioned earlier, the 2a and 4b sites (figure 3) have point symmetries $3m$ (C_{3v}) and 3 (C_3) respectively. Using the Stevens notation [20], the CF Hamiltonian for the trigonal symmetry of the Tm 4b site is represented by

$$\mathcal{H}_{CF} = B_2^0 O_2^0 + B_4^0 O_4^0 + B_4^3 O_4^3 + B_4^{-3} O_4^{-3} + B_6^0 O_6^0 + B_6^3 O_6^3 + B_6^{-3} O_6^{-3} + B_6^6 O_6^6 + B_6^{-6} O_6^{-6}. \quad (3)$$

Point charge model estimates of the CF parameters, B_n^m, were carried out using the lattice parameters and atomic position parameters reported by Uusi-Esko *et al* [9]. The CF x- and z-axes were set to align with the a- and c-axes, respectively and the point charges were taken as Tm^{3+}, Mn^{3+} and O^{2-}. The summation was found to converge over a sphere of radius $r > 50\ a$ and the resulting estimates are listed in the first column of table 1. The second column represents the parameters after a rotation of the coordination axes through $\chi = \frac{1}{3}\tan^{-1}(B_4^{-3}/B_4^3)$ about the c-axis to give a zero value for B_4^{-3}. It is interesting that the transformation also results in greatly reduced values of B_6^{-3} and B_6^{-6}. This supports the assumption that the adoption of a CF Hamiltonian for the higher C_{3v} symmetry of the 2a site is also a reasonable approximation for the 4b site, as assumed earlier for h-$YbMnO_3$ by Diviš *et al* [13]. The B_n^m values presented in the third column of table 1 have been converted from those reported by Diviš *et al* [13] for h-$YbMnO_3$ using the assumption that

$$B_n^m(Tm^{3+}) = B_n^m(Yb^{3+})\frac{[\theta_n(1-\sigma_n)\langle r^n\rangle]_{Tm^{3+}}}{[\theta_n(1-\sigma_n)\langle r^n\rangle]_{Yb^{3+}}} \quad (4)$$

where the symbols have their usual meanings [20] with values taken from Gupta and Sen [21] and Freeman and Desclaux [22]. In general, the converted values differ from the PCM estimates by factors of about 2/3 for $n = 2$ and about 4 for $n = 6$.

Using the set of B_n^m converted as a useful starting point, the CF scheme for the Tm^{3+}, $^3H_6$ multiplet at the 4b site is calculated to be as shown in figure 5. The most important aspect of this scheme is that there is a well-isolated two-singlet ground state. Given that the singlet states are non-magnetic, the inducement of a net Tm^{3+} magnetic moment on the 4b site requires that the molecular field associated with the weak Mn–Tm exchange interaction brings about a mixing of these levels. Under these circumstances, the induced magnetic moment is given by

$$\mu(Tm) = \frac{2g_J^2\mu_B^2\alpha^2 B_M}{\Delta'}\tanh\left(\frac{\Delta'}{2k_BT}\right) \quad (5a)$$

where B_M is the molecular field acting in the z-direction (parallel to the crystallographic c-axis), $\alpha = \langle 0|J_z|1\rangle$ is the J_z coupling parameter between the two singlets and

$$\Delta' = \left[\Delta^2 + (2g_J\mu_B\alpha B_M)^2\right]^{\frac{1}{2}} \quad (6)$$

is the field-enhanced energy separation of the two singlets (Δ is the energy separation in the absence of a molecular field).

In order to arrive at a theoretical estimate of the induced moment, it was assumed that the molecular field acting at the 4b site is proportional to the Mn moment. In turn, this was assumed to have a temperature dependence described by the empirical formula employed elsewhere by Lonkai *et al* [23]

$$B_{\mathrm{hf}} = B_{\mathrm{hf}}(T=0) = \left(1 - \left(\frac{T}{T_{\mathrm{N}}}\right)^{\alpha'}\right)^{\beta'} \tag{7}$$

with parameters $\alpha' = 2.6$ and $\beta' = 0.27$, as determined by Salama *et al* [14] for h-$YbMnO_3$. The only parameters remaining to be determined were then the saturation value of the molecular field, $B_M(T = 0\ \mathrm{K})$ and the two-singlet state parameters Δ and α.

The theory curve (solid line) drawn through the experimental data in figure 4 corresponds to the values of $B_M(T = 0\ \mathrm{K}) = 1.27(1)$ T, $\Delta = 20.2(2)$ K and $\alpha = 6.00(2)$ K, where the uncertainties are based on the range of acceptable variation with the other two parameters fixed. It is evident that the form of the theory curve matches closely with the temperature dependence of the experimental data, despite only three parameters being allowed to vary. This provides strong support for the simple theoretical model that has been adopted. However, the solution is not unique. If the value of α is reduced, then an alternative fit can be achieved with an appropriate reduction of Δ and an increase in $B_M(T = 0\ \mathrm{K})$. For example, the tentative CF Hamiltonian predicts that $\alpha \approx 4.5$ and a similar quality theory curve can then be found with $\Delta \approx 17$ K and $B_M(T = 0\ \mathrm{K}) \approx 2.25$ T. This ambiguity can be resolved only with an improved experimental characterization of the CF interaction.

5. Concluding remarks

In conclusion, ^{169}Tm Mössbauer spectroscopy has proved to be a useful tool for monitoring the exchange-induced magnetization at the Tm 4b site in h-$TmMnO_3$. Analysis of the experimental data confirmed that the Mn sublattice orders magnetically below $T_{\mathrm{N}}^{\mathrm{Mn}} = 82$–$83$ K and that the Mn–Tm exchange interaction acts only at the rare earth 4b site. Finally, a simple two-singlet CF ground state model has been demonstrated to provide a close description of the temperature dependence of the magnetic hyperfine field recorded at the ^{169}Tm nucleus (and hence the induced Tm^{3+} moment) at the Tm 4b site.

Acknowledgments

Hazar Salama gratefully acknowledges her University International Postgraduate Award, University College Postgraduate Research Scholarship, and additional financial support from the School of PEMS. The neutron activations of the ^{169}Tm Mössbauer source were carried out at the Australian OPAL Reactor (AINSE Grant 2008/60).

References

[1] Yakel H L, Koehler W C, Bertaud E F and Forrat E F 1963 *Acta Crystallogr.* **16** 957–62
[2] Huang Z L, Cao Y, Sun Y Y, Xue Y Y and Chu C W 1997 *Phys. Rev.* B **56** 2623–6
[3] Park J, Park J-G, Jeon G S, Choi H Y, Lee C, Jo W, Bewley R, McEwen K A and Perring T G 2003 *Phys. Rev.* B **68** 104426
[4] Fiebig M, Lottermoser Th and Pisarev R V 2003 *J. Appl. Phys.* **93** 8194–6
[5] Fabrèges X, Mirebeau I, Bonville P, Petit S, Lebras-Jasmin G, Forget A, André G and Pailhès S 2008 *Phys. Rev.* B **78** 214422
[6] Salama H A, Voyer C J, Ryan D H and Stewart G A 2009 *J. Appl. Phys.* **105** 07E110
[7] Yen F, dela Cruz C, Lorenz B, Galstyan E and Sun Y Y 2007 *J. Mater. Res.* **22** 2163–73
[8] Zhou J-S, Goodenough J B, Gallardo-Amores J M, Morán E, Alario-Franco M A and Caudillo R 2006 *Phys. Rev.* B **74** 014422
[9] Uusi-Esko K, Malm J, Imamura N, Yamauchi H and Karppinen M 2008 *Mater. Chem. Phys.* **112** 1029–34
[10] Howard C J and Hunter B A 2000 *Rietica* available from http://www.ccp14.ac.uk
[11] Wang L J, Feng S M, Zhu J L, Yu R C and Jin C Q 2006 *Phys. Rev.* B **74** 014422
[12] Kritayakirana K, Berger P and Jones R V 1969 *Opt. Commun.* **1** 95–8
[13] Diviš M, Hölsä J, Lastusaari M, Litvinchuk A P and Nekvasil V 2008 *J. Alloys Compounds* **451** 662–5
[14] Salama H A, Stewart G A, Ryan D H, Elouneg-Jamroz M and Edge A V J 2008 *J. Phys.: Condens. Matter* **20** 255213
[15] Wit H P and Niesen L 1976 *Hyperfine Interact.* **1** 501–4
[16] Bauminger E R, Kalvius G M and Nowik I 1978 *Mössbauer Isomer Shifts* ed G K Shenoy and F E Wagner (Amsterdam: North-Holland) p 661
[17] Stone N J 2005 *At. Data Nucl. Data Tables* **90** 75–176
[18] Stewart G A 1994 *Mater. Forum* **18** 177–93
[19] Stewart G A, Day R K, Dunlop J B and Price D C 1988 *Hyperfine Interact.* **40** 339–42
[20] Stewart G A 1985 *Hyperfine Interact.* **23** 1–16
[21] Gupta R P and Sen S K 1973 *Phys. Rev.* A **7** 850–8
[22] Freeman A J and Desclaux J P 1979 *J. Magn. Magn. Mater.* **112** 11
[23] Lonkai Th, Hohlwein D, Ihringer J and Prandl W 2002 *Appl. Phys.* A **74** (Suppl.) S843–5